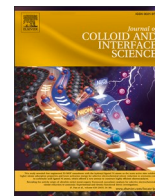




Contents lists available at ScienceDirect

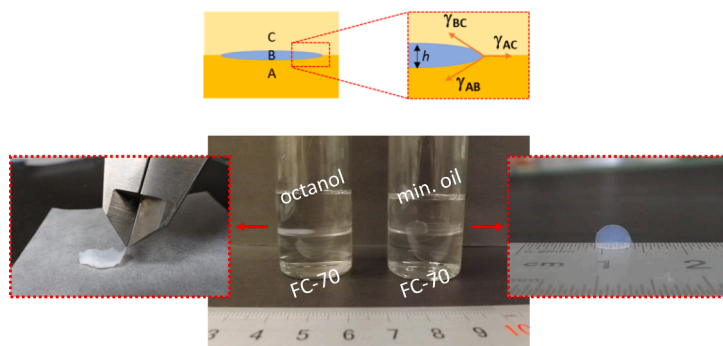
Journal of Colloid And Interface Science

journal homepage: www.elsevier.com/locate/jcis

Synthesis of silica aerogel films in liquid molds

Galit Bar^{a,c,*}, Linoy Amar^a, Michal Marszewski^{c,f}, Assaf Bolker^b, Ali Dashti^c, Raphy Dror^a, Laurent Pilon^{c,d,e}^a Applied Physics Department, Soreq Nuclear Research Center, Yavne 81800, Israel^b Space Environment Department, Soreq Nuclear Research Center, Yavne 81800, Israel^c Mechanical and Aerospace Engineering Department, Henry Samueli School of Engineering and Applied Sciences, University of California Los Angeles, Los Angeles, CA 90095, USA^d California NanoSystems Institute, University of California Los Angeles, Los Angeles, CA 90095, USA^e Institute of the Environment and Sustainability, University of California Los Angeles, Los Angeles, CA 90095, USA^f Department of Chemistry and Biochemistry, University of Toledo, Toledo, OH 43606, USA

GRAPHICAL ABSTRACT



ARTICLE INFO

Keywords:

Sol-gel
Silica aerogel
Floating aerogel
Liquid mold
Aerogel film
Free-standing film
Controlled evaporation
Liquid encapsulation

ABSTRACT

By virtue of their low density and thermal conductivity, aerogels constitute attractive thermal insulators. Of those, aerogel films are best suited for thermal insulation in microsystems. Processes for the synthesis of aerogel films with thicknesses smaller than 2 μm or thicker than 1 mm are well established. However, for microsystems films in the range of a few microns and up to several hundred microns would be beneficial. To circumvent the present limitations, we describe a liquid mold made of two immiscible liquids, used here to produce aerogel films thicker than 2 μm in a single molding step. Following gelation and aging, the gels were removed from the liquids and dried using supercritical carbon dioxide. In contrast to spin/dip coating, liquid molding avoids solvent evaporation from the gel's outer surface during gelation and aging, films are free-standing and have smooth surfaces. The choice of liquids determines the aerogel film thickness. As a proof of concept, 130 μm thick

Abbreviations: BET, Brunauer–Emmett–Teller (theory for surface area analysis); BJH, Barrett–Joyner–Halenda (theory for pore size distribution calculation); CO_2 , Carbon dioxide; CPD, Critical Point Drying; ϕ , Porosity; g , Gravitational acceleration; h , Film thickness; IR, Infrared; KJS, Kruk–Jaroniec–Sayari (correction method for pore size analysis); MEMS, Microelectromechanical systems; NMP, *N*-methyl 2-pyrrolidone; PSD, Pore Size Distribution; ρ , Density; ρ_a , Apparent density; ρ_s , Density of silica; SEM, Scanning Electron Microscopy; S , Spreading coefficient; TEOS, Tetraethyl orthosilicate; UV–Vis, Ultraviolet–Visible; V_p , Pore volume; W_p , Pore width.

* Corresponding author at: Applied Physics Department, Soreq Nuclear Research Center, Yavne 81800, Israel.

E-mail address: gali@soreq.gov.il (G. Bar).

<https://doi.org/10.1016/j.jcis.2023.06.004>

Received 12 January 2023; Received in revised form 8 May 2023; Accepted 1 June 2023

Available online 7 June 2023

0021-9797/© 2023 Elsevier Inc. All rights reserved.

homogeneous and high porosity (>90%) silica aerogel films were synthesized in a liquid mold with fluorine oil and octanol. The resemblance of the liquid mold approach to the float glass technique offers the prospect of mass production of large sheets of aerogel films.

1. Introduction

Aerogels are highly porous solid materials, with porosities over 90%, known for their high surface area and excellent thermal insulation properties [1,2]. The thermal conductivity of aerogels can be as low as $10 \text{ mW}\cdot\text{m}^{-1}\cdot\text{K}^{-1}$ under ambient conditions [3]. Aerogel powders and large aerogel monoliths are commercially available in applications such as thermally insulating blankets [4] and skylight windows [5,6]. To the best of our knowledge, aerogel films, less than 1 mm in thickness, are not produced industrially despite their potential use in multilayered integrated circuits [7,8] and as gas–liquid barriers in microsystems [9]. Aerogel films can also be used in microelectromechanical systems (MEMS) as micro bridges, cantilevers, and membranes [10,11]. They can also be incorporated in high-sensitive humidity sensors [12]. The limited use of aerogel films can be attributed to the difficulties associated with their synthesis.

Aerogels made by the sol–gel technique involve the preparation of a gel from a solution of suspended solid nanoparticles (named sol) [13]. The particles can be synthesized from metal alkoxides through a sequence of hydrolysis and condensation reactions. As condensation proceeds, a continuous and complex network of metal oxide nanoparticles forms a gel featuring mesoscale open pores (2–50 nm wide). The gel is very sensitive to ambient drying due to strong capillary pressure prevailing inside the pores [14]. To preserve the porosity and mechanical integrity of the gel, drying is performed under supercritical conditions [15]. In fact, solvent evaporation under ambient conditions results in shrinkage and sometimes cracking of the solid skeleton [16]. This problem is exacerbated in the synthesis of aerogel films when the external surface-to-volume ratio is very large.

Previous attempts to produce thin aerogel films included dip coating, spin coating, and spray coating of the sol on a solid substrate followed by supercritical drying [17–19]. To overcome the challenges posed by ambient evaporation from the freshly formed thin gel, a solvent-saturated environment was imposed during the film deposition and maintained after the gel formation to reduce the evaporation rate [17]. However, this approach limits the sample size due to the enclosure necessary to maintain the proper atmospheric composition. In addition, the film thickness in spin and dip coating processes is limited to tens of nanometers up to a few microns [18]. In order to achieve larger thicknesses, the film deposition process can be repeated multiple times [10,11]. However, multilayer spin-coated or dip-coated films are limited to a few microns in thickness (<2 μm) due to the penetration of the solution into the previously deposited layers resulting in non-uniform layers with different thicknesses and porosities. In addition, “coating” techniques produce films strongly bonded to the solid substrate and are therefore not suitable for producing free-standing aerogel films.

The float glass process is a well-known technique to manufacture large and flat sheets of glass by pouring molten glass on a bath of hot liquid tin [20]. It can produce glass sheets with uniform thickness and optically smooth surfaces. It is widely used to produce architectural and automobile glass products and flat panel displays [21]. The float glass process has been adapted to sol–gel chemistry by using poly(chlorotrifluoroethylene) [22] and perfluoropolyether oil [23] as liquid substrates for producing free-standing mesoporous silica slabs. In both cases, the immiscible liquid substrate was used as an intermediate layer in solid containers. Its role was to eliminate friction with the container due to shrinkage of the gel during drying and to obtain optically smooth surfaces.

Interfacial polymerization consists of forming a thin solid film via chemical reactions at the interface between two immiscible but reacting

liquids [24]. It has been demonstrated for silica sol–gel at the interface between hexane and water containing ammonium hydroxide [25]. The film thickness depends on the concentration and diffusion rate of the silica oligomers. It can range from 2 to 20 μm but it is difficult to control.

Moreover, liquid encapsulation has been used for protein crystal growth in protein characterization [26,27]. Briefly, an aqueous solution of protein is injected between two layers of immiscible oils with different densities. The water evaporates slowly from the confined aqueous solution through the top oil layer while a crystal of the protein grows. This technique captures the advantage of growing protein crystals with a perfect crystalline structure ascertained by preventing direct contact of the protein solution with the container walls, which often act as a heterogeneous nucleation site for crystal growth.

Here we report on a novel method to synthesize free-standing aerogel films with thickness > 100 μm in one molding step using liquid encapsulation. This approach combines principles reminiscent of the float glass, interfacial polymerization, and encapsulated crystallization. The structure and thickness of silica aerogel films obtained in the liquid mold technique were characterized by nitrogen porosimetry and scanning electron microscopy (SEM). Their transmittance and haze were measured across the visible part of the spectrum. The low thermal conductivity of the films was validated by thermal imaging when they were placed on a hotplate. The liquid mold method was demonstrated for silica-based aerogels due to their wide range of applications but it could be extended to aerogels of other material compositions.

2. Experimental

2.1. Materials

Chemicals for the gel preparation were used as received and included (i) 99% tetraethyl orthosilicate (TEOS) from Sigma-Aldrich, (ii) absolute ethanol dehydrated (extra dry, $\geq 99.5\%$) from Bio-Lab, (iii) ammonium fluoride ($\geq 99.99\%$) and (iv) ammonium hydroxide (28–30% wt, $\geq 99.99\%$) from Sigma-Aldrich, and (v) distilled water. Supercritical drying was performed with dry acetone ($\geq 99.9\%$) purchased from Bio-Lab and liquid CO_2 with > 99% purity.

Liquids used for the molds as substrates were (i) fluorinated oil perfluoropolyether, trade name Fomblin® Y25 by Solvay (100%), (ii) Fluorinert™ (FC-70) from Synquest Laboratories ($\leq 100\%$), (iii) glycerol from Fluka (anhydrous, >99.5%), (iv) ethylene glycol from Sigma-Aldrich (anhydrous, 99.8%), (v) *N*-methyl 2-pyrrolidone (NMP) from Sigma-Aldrich (anhydrous, >99.5%), and (vi) silicone oil from Sigma-Aldrich (350cSt). As covers: (vii) mineral oil also known as paraffin oil from Sigma (bioreagent), and (viii) octanol from Thermo Fisher (99%). All the liquids were used as received without further treatment.

2.2. Gel preparation

Silica gels were prepared from TEOS using a one-step base-catalyzed recipe [28]. First, a catalyst solution was made by mixing 0.74 g ammonium fluoride, 8.20 g of 30 wt% ammonium hydroxide, and 40 ml distilled water. Then, two solutions were prepared in separate beakers, one containing 2.62 g ethanol and 1.42 g TEOS, and the other containing 2.62 g ethanol, 2.16 g distilled water, and 0.11 g of the catalyst solution. The solutions were mixed separately for a few minutes and then combined. The final molar ratio of TEOS, water, and ethanol was 1:16.7:18.7, respectively. The resulting mixture was stirred for 1 min and then applied dropwise onto the liquid mold (described in detail in section 2.3. *Liquid molds*). Gelation occurred after 9–12 min. Gels were

left in the liquid mold for about 1 h and then transferred into an ethanol bath under ambient conditions. To maintain the integrity of the films a stainless-steel mesh was used to support the gels during the transfer and in the ethanol bath. The gels were immersed in ethanol to age for a day before undergoing supercritical drying.

2.3. Liquid molds

The liquid molds consisted of two immiscible liquids. Liquids with a density larger than that of the silica sol sat at the bottom and served as the substrate. Liquids with a density lower than that of the silica sol served as the cover. In addition to density and miscibility, properties such as vapor pressure, and surface tension also determined whether a liquid could serve as substrate or cover. Specifically, low vapor pressure is important for the cover liquid to minimize evaporation and to maintain full coverage of the sol and gel throughout the duration of the synthesis. Densities and vapor pressures at room temperature were obtained from either the literature [29] or suppliers. The miscibility of liquids was tested by “mixing” pairs of liquids in a glass beaker and observing (or not) the formation of a clear interface. The interface was examined over a few days at ambient conditions.

To assemble the liquid mold, the liquid cover was gently poured on top of the liquid substrate in a glass beaker. The liquids were left for a few minutes to settle before introducing the sol. The sol was applied dropwise close to the top of the cover liquid. Due to density differences, the sol passed through the cover liquid until it settled on top of the liquid substrate. Fig. 1(a) shows a photograph illustrating the layered structure of a liquid mold with silica gel confined between fluorinert as the liquid substrate and mineral oil as the liquid cover.

The thickness h of sol suspended in the liquid mold and isolated from the container walls was determined by the surface tension forces acting at the interfaces of the three liquids [30], as illustrated in Fig. 1(b). The net balance of the surface tension forces corresponds to the spreading coefficient S , which is defined as [31]

$$S = \gamma_{AC} - (\gamma_{AB} + \gamma_{BC}) \quad (1)$$

where γ_{ij} is the surface tension of the interface separating liquids “i” and “j”, while subscripts A, B, and C refer to the liquid substrate, the sol, and the liquid cover, respectively. When the spreading coefficient $S > 0$, the sol spreads on the liquid substrate and forms a thin layer (complete wetting) [32]. By contrast, when $S < 0$, the sol forms lens shaped film [33] whose thickness h depends on the spreading coefficient, the gravitational acceleration, g , and the differences between the densities of the liquids in the system. The square of h is derived from the Langmuir equations [34,35] and is given by the expression

$$h^2 = -2S \frac{\rho_A - \rho_C}{g(\rho_A - \rho_B)(\rho_B - \rho_C)} \quad (2)$$

where ρ_A , ρ_B and ρ_C refer to the densities of the liquids as they are defined in equation (1) and in Fig. 1(b). Since the liquids are layered from bottom to top by order of decreasing densities, the product of the density differences is always positive. Therefore, when the value of S approaches zero the films obtained are thinner. In addition, when the volume of the sol is equal to or smaller than $\frac{1}{6}\pi h^3$ (the volume of a sphere in terms of its diameter h) spherical beads are obtained.

Another important aspect of the liquid mold is to ensure the planarity of the interfaces between liquids in the solid container. Due to the surface tension between the liquids and the solid container wall, the liquid interfaces are nonplanar near the wall. To minimize this effect a wide container was used [36]. This provided horizontal interfaces at the center where the gel film was produced [37].

Finally, most liquids of the mold were recovered after the synthesis and were reused in subsequent experiments.

2.4. Supercritical drying

After removing the silica gels from the liquid mold and aging, supercritical drying was performed in a Leica CPD300 or a Tousimis Automegasamdri 915B critical point dryers. First, the drying cell was partially filled with acetone, and the gels were transferred from the ethanol bath to the drying cell. Acetone was used because it is more miscible with CO₂ than ethanol. After closing the drying cell, it was cooled to 6 °C at atmospheric pressure. Then, the drying cell was filled with liquid CO₂ at about 58 bars while maintaining a low temperature. Between 10 and 100 exchange cycles were performed to fully remove the acetone and ethanol. Each cycle included flush out of about 10% of the liquid mixture followed by insertion of liquid CO₂ to fill the empty volume and mixing for about 4–5 min. Following the exchange cycles, the cell was slowly heated to 43 °C at a rate of 1.5 °C·min⁻¹ while the pressure increased to 78 bars (1131 psi). Supercritical conditions were maintained for several minutes before starting a slow depressurization at 40–43 °C. After the pressure was released the cell was left to cool down ambiently.

2.5. Characterization

The density of the sol was measured at room temperature by monitoring mass and volume of the sol from the time of mixing until a solid gel was formed. The density of the dry aerogel films ρ_a was obtained from the weight, and size which were measured using a balance, and “ImageJ” software (version 1.52v) [38] with the ‘analyze → measure’ function. Thicknesses of films (<1 mm) were measured with a SEM or confocal laser microscope. The total porosity ϕ was calculated from the apparent density of the sample ρ_a and the density of silica $\rho_s = 2.2 \text{ g}\cdot\text{cm}^{-3}$ according to equation (3) [39]

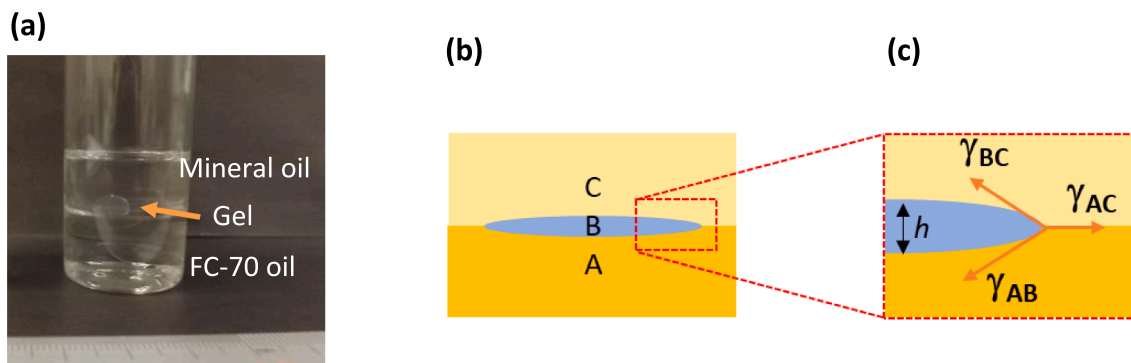


Fig. 1. (a) Stratified structure of a silica gel in a liquid mold with fluorinert (FC-70) as the liquid substrate and mineral oil as the liquid cover. (b) Schematic illustration of a sol or gel, B, at the interface between a liquid substrate, A, and a liquid cover, C. (c) Surface tension force vectors, γ_{ij} , and the thickness, h , of the gel are depicted in the scheme, which is a magnified view of the highlighted rectangle in (b).

$$\phi = 1 - \frac{\rho_a}{\rho_s} \quad (3)$$

The total pore volume V_p (in $\text{g}\cdot\text{cm}^{-3}$) was calculated according to equation (4)

$$V_p = \frac{1}{\rho_a} - \frac{1}{\rho_s} \quad (4)$$

and is equal to the sum of volumes from micropores, mesopores, and macropores.

The dry free-standing silica aerogel films were characterized using (i) SEM, (ii) low-temperature nitrogen adsorption–desorption porosimetry, and (iii) UV–vis spectrometry. SEM characterization was performed using a Zeiss Sigma 300 VP scanning electron microscope. Free-standing films were glued to SEM stubs using carbon tape. The stubs were inserted into the SEM and evacuated for about 2 h until a high vacuum was reached. This also enabled the aerogel samples to equilibrate with the conditions in the SEM vacuum chamber. It was previously shown that even a thin layer of sputtered gold, dramatically alters the morphology and the fine structure of aerogels [40], therefore, SEM measurements were performed on samples without coating. To overcome the charging effect a relatively low-energy electron beam (3 keV) was applied. In addition, a low-diameter aperture was used (15 μm), thereby reducing the beam current.

A 3D-measuring laser confocal microscope (LEXT OLS5100, Olympus) was used to acquire the vertical cross-section of the aerogel films. At 405 nm in ‘Film thickness’ scanning mode, the laser light was able to image the uniformity and homogeneity of the material. The thickness of the films was evaluated by the microscope ‘Analysis Application’, (version 1.3.4.170, 2017) in a $10\times$ magnification and $1\times$ zoom.

A Micromeritics Tri-Star II surface area and porosity analyzer was used to examine the specific surface area, pore structure, and porosity of the aerogel films. A VacPrep061 sample degas system by Micromeritics was used for degassing the samples prior to the measurements. Several films prepared in liquid molds as described above were collected after gelation and combined in a stainless-steel mesh basket and then dried under supercritical conditions. About 50 mg of the dry films were loaded in a narrow-neck glass test tube for degassing and measurement. Degassing was performed at 150 °C for 20.5 h. Measurements were repeated several times to verify their reliability. Surface area and pore structure were calculated from low temperature nitrogen adsorption–desorption isotherms based on the Brunauer–Emmett–Teller (BET) algorithm [41,42] and the Barrett–Joyner–Halenda (BJH) Analysis [43] with Kruk–Jaroniec–Sayari (KJS) correction [44,45]. The pore size distribution (PSD) is represented by the differential ratio of pore volume, V_p , and pore width, W_p , as a function of the pore width. Micropore and mesopore volumes were calculated using the α_s comparative plot method [46].

The spectral normal-hemispherical transmittance and haze of the aerogel films were measured using a double-beam ultraviolet–visible (UV–Vis) spectrophotometer (iS50, Thermo Fisher Scientific, USA) equipped with an integrating sphere (EVO220, Thermo Fisher Scientific, USA), as described in ASTM D1003-11 [47]. Measurements were performed in the visible and near-infrared range between 300 and 1100 nm in 1 nm increments. The films were held by electrostatic forces on a polystyrene slide during the measurements. Absorption by the slide was subtracted from the spectra.

The thermal insulation performance of the aerogel films was demonstrated with an infrared (IR) camera FLIR A320.

3. Results and discussion

3.1. Synthesis design

The density of the sol dictates the choice of liquids that can serve as substrate or cover in the mold. Here, the density of silica sol was

measured as $0.90 \pm 0.01 \text{ g}\cdot\text{cm}^{-3}$ and it remained constant during gelation. Liquid densities and miscibility tests established that silicone oil, NMP, benzyl alcohol, ethylene glycol, glycerol, and fluorinated oils can be used as liquid substrates. Similarly, liquids suitable to serve as liquid covers include octanol and mineral oil. All the liquids listed above were tested and found to be immiscible with the silica sol and formed an intact gel.

The use of some liquids resulted in very smooth surfaces while others led to textured surfaces. Surface smoothness is critical for several applications such as thermal insulation in multi-layered microelectronics, where smooth surfaces improve device compactness and avoid complications due to the presence of air pockets [48,49]. Fig. 2 shows $2 \times 2 \text{ mm}^2$ microscope images of dry silica aerogel surfaces obtained in contact with different liquids. The surfaces of aerogels obtained with fluorinated oil and silicone oil as substrates, and mineral oil as a cover were perfectly smooth, comparable to the surface of the same aerogel formed under air. Liquids such as benzyl alcohol, NMP, glycerol, and ethylene glycol, which were used as substrates, caused the formation of different patterns on the surface. Such roughness is incompatible with applications where surface smoothness is critical and compact layering is required.

The surface tension between the mold liquids and the sol determines the thickness of the resulting gel, as shown in equation (2). In a liquid mold with silicone oil as a substrate and mineral oil as a cover, lens shaped aerogels with thickness $\sim 4 \text{ mm}$ after supercritical drying were obtained due to high surface tension, Fig. 3(a). Small volumes of sol, less than 35 μl , in the same liquid mold, resulted in spherical aerogel beads $\sim 4 \text{ mm}$ (or smaller) in diameter, as shown in Fig. 3(b). Similar results were obtained in references [50,51]. Accordingly, the spreading coefficient for this mold, calculated from equation (2) for the silica sol, was negative and equal to $-2.53 \text{ mN}\cdot\text{m}^{-1}$. Attempts to reduce the gel thickness in this mold included (i) withdrawing the sol after deposition [22] (ii) heating the liquid mold up to 40 °C, and (iii) using a thick layer of liquid cover to increase the hydrostatic pressure forces on the gel. All the above approaches had negligible effect on the gel thickness.

Thin aerogel films were obtained in a liquid mold with fluorinert as a substrate and octanol as a cover. The polarity of octanol lowered the surface tension with the sol resulting in a larger spreading coefficient (less negative). Fig. 4(a) presents a small segment of a silica aerogel film made in a liquid mold with fluorinert and octanol. The thickness of the dry film was measured by SEM to be about 160 μm , as illustrated in Fig. 4(b). Since the SEM measurement represents only the edge of the film, a laser confocal microscope was used to measure the vertical cross-section of the film at its center. The images revealed a film thickness equal to $130 \pm 10 \mu\text{m}$, see image 4(d), and accordingly, the spreading coefficient calculated for this mold is $-0.006 \text{ mN}\cdot\text{m}^{-1}$. Due to the dispersive nature of the aerogels, the light intensity across the film decreased as it penetrated deeper into the film (from top to bottom). Therefore, the bottom side of the film appears darker.

Production of large flat films in the liquid mold was challenging due to vibrations and small movements of the surroundings and of the liquid interfaces. A flat gel film $\sim 10 \text{ cm}$ in diameter was successfully produced in a large container. However, maintaining the integrity and flatness of such film (or larger) requires a vibration control platform during gelation and a stable support when being transferred from the mold to the drying cell. Here the large film was sectioned before it was transferred to the drying cell. Notably, supercritical drying of a large film requires control of the inlet stream or other measures to protect the gel from destructive currents during the solvent exchange.

3.2. Structural characterization

The apparent density ρ_a and the total porosity ϕ of the silica aerogel films synthesized in liquid molds consisting of fluorinert and octanol were calculated directly from the weight and size, and found to be 190

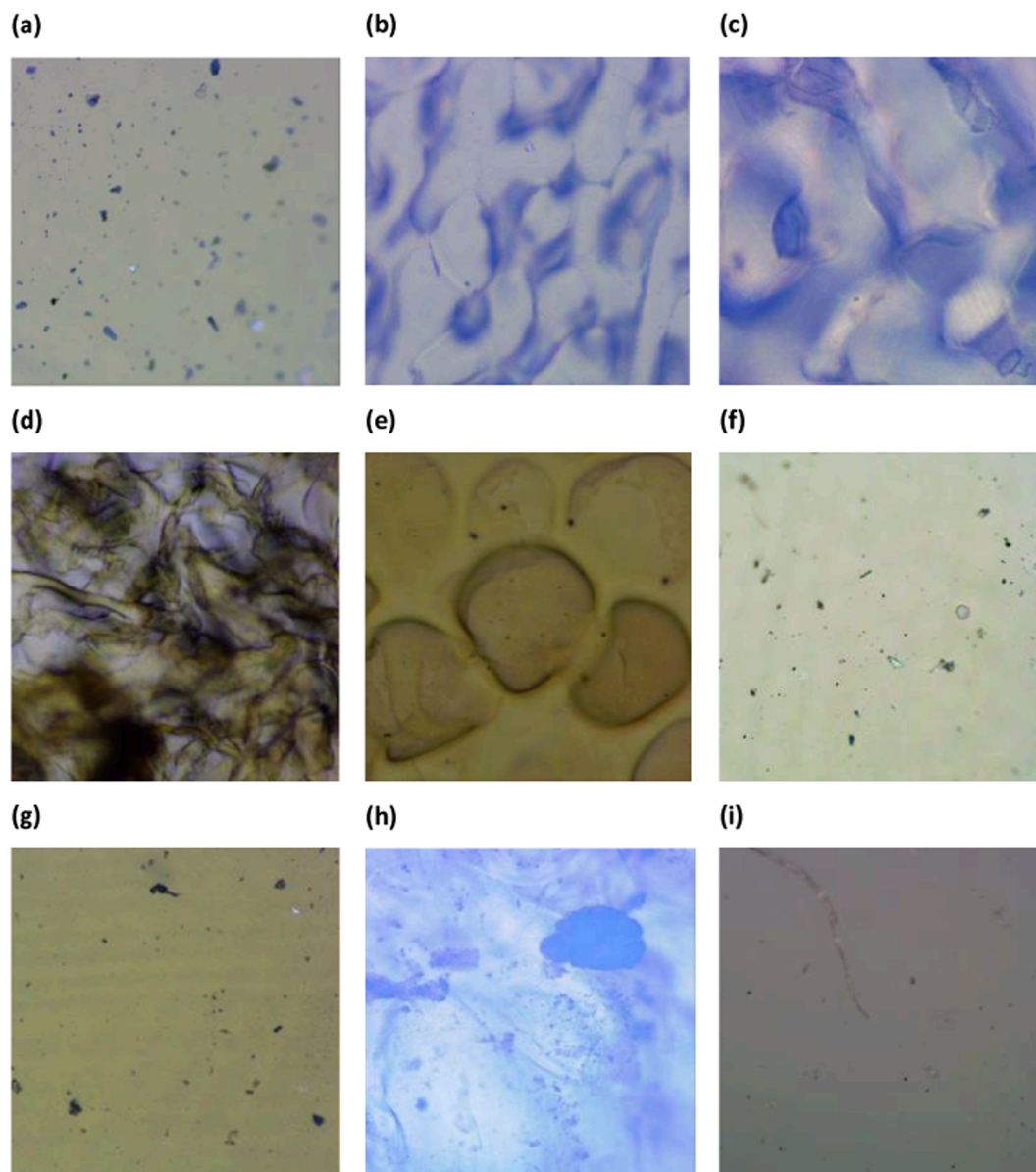


Fig. 2. Optical microscope images ($2 \times 2 \text{ mm}^2$) of aerogel surfaces that were synthesized in contact with different liquids. High density liquids used as substrates: (a) fluorinated oil Fomblin™, (b) glycerol, (c) ethylene glycol, (d) benzyl alcohol, (e) NMP, (f) silicone oil; Low density liquids that were used as cover liquids: (g) mineral oil and (h) octanol. A reference sample with interface obtained under air is shown in (i).

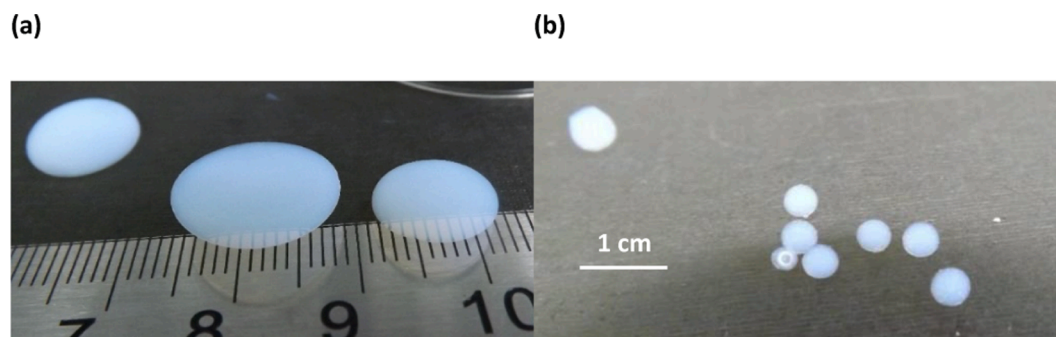


Fig. 3. Photographs of silica aerogels synthesized in a liquid mold of silicone oil as the substrate and mineral oil as the cover, and dried in supercritical CO_2 . (a) Lens-shaped aerogels with thickness equal to 4 mm were obtained when sol volumes were larger than $35 \mu\text{l}$; (b) Small volumes of sol, $\leq 35 \mu\text{l}$, generated spherical aerogel beads with diameters $\sim 4 \text{ mm}$ or less.

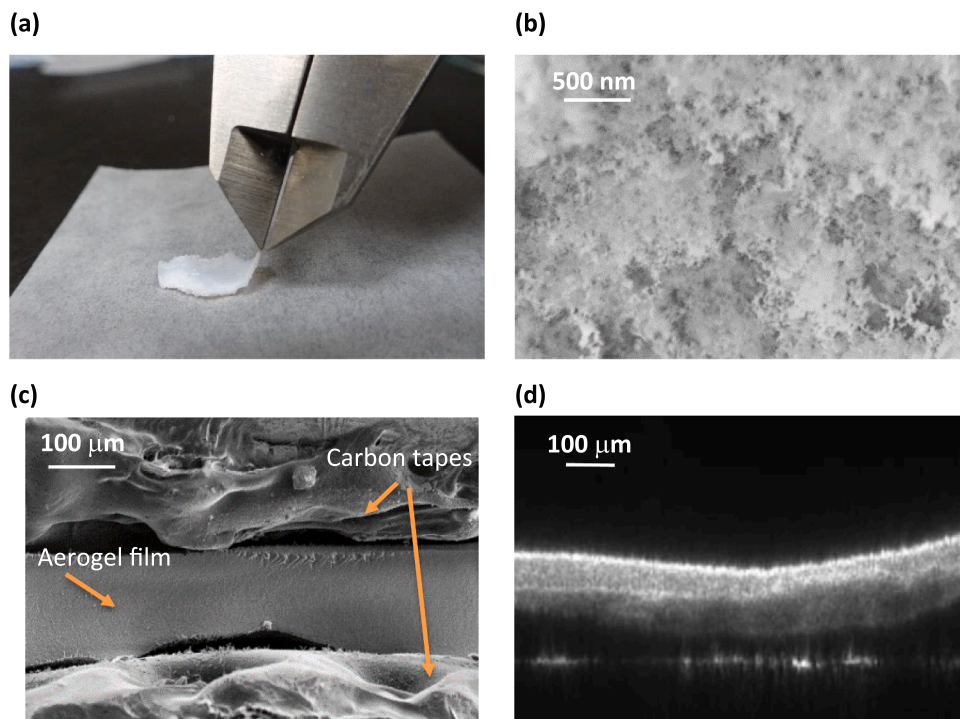


Fig. 4. (a) Photograph of a silica aerogel film synthesized in a liquid mold of fluorine oil Fomblin as the substrate and octanol as the cover, and dried in supercritical CO_2 . Film is shown under the tip of a caliper. (b) SEM picture of the aerogel film shows its porous structure. (c) SEM picture of the cross-section of the film was taken at low magnification while the film was held by carbon tapes on both sides. (d) Laser scanning microscope image of the aerogel film showing the uniformity, homogeneity and thickness.

$\pm 10 \text{ mg}\cdot\text{cm}^{-3}$ and 91%, respectively.

The SEM picture presented in Fig. 4(c) displays the porous structure of the film. Mesopores and macropores are qualitatively observed in the picture. Gas adsorption–desorption analysis was used to further examine the porous structure of the material. Fig. 5(a) shows a representative nitrogen adsorption–desorption isotherm of the aerogel film. The isotherm consists a steep increase at a low relative pressure and a hysteresis loop that does not reach a plateau at a relative pressure close to 1. These features indicate a mixture of type II and type IV(a) isotherms, according to the International Union of Pure and Applied Chemistry (IUPAC) classification [52]. The hysteresis loop is related to the presence of mesopores (2–50 nm), while the lack of plateau at $P/P_0 \approx 1$ is attributed to the presence of macropores (>50 nm). The latter is also consistent with the type H3 hysteresis loop, which is observed in mesopore systems with macropores. Fig. 5(b), shows the mesopore size distribution calculated by the BJH-KJS method, which demonstrates a broad distribution of pores from 2 to over 50 nm, and potential presence of micropores (<2 nm) and macropores (>50 nm). The α_s comparative plot method was used to calculate the volumes of micropores and mesopores. However, PSD integration was not used to calculate the total mesopore volume as the presence of macropores adversely affects the accuracy of the PSD calculations. The micropore and mesopore volumes calculated by the α_s method were 0.05 and $0.40 \text{ cm}^3\cdot\text{g}^{-1}$, respectively. The macropore volume of $4.36 \text{ cm}^3\cdot\text{g}^{-1}$ was calculated by subtracting the micropore and mesopore volumes from the total pore volume of $4.81 \text{ cm}^3\cdot\text{g}^{-1}$. Table 1 summarizes the structural characteristics of the aerogel films. The results indicate that the aerogel films synthesized in the liquid mold with fluorinert and octanol were predominantly macroporous and that the PSD shown in Fig. 5(b) accounts only for a fraction of the pores.

The specific surface area of the film, calculated from the slope of the linear regime at low relative pressures was equal to $430 \pm 9 \text{ m}^2\cdot\text{g}^{-1}$. In comparison, a large silica aerogel monolith 20 mm in diameter and 5 mm in thickness synthesized by the same procedure as that of the films in liquid molds but in a solid Teflon mold had specific surface area of $850 \text{ m}^2\cdot\text{g}^{-1}$, effective density of $70 \text{ mg}\cdot\text{cm}^{-3}$, and porosity of 0.97 [53].

Therefore, we conclude that the liquids constituting the mold affected the microstructure of the silica aerogel, increasing the pore size and reducing the surface area.

3.3. Optical characterization

Fig. 6 shows the measured spectral normal-hemispherical transmittance and haze of a $130 \mu\text{m}$ thick silica aerogel film synthesized in a liquid mold consisting of fluorinert and octanol. The large haze confirms the existence of large pores in line with the nitrogen adsorption–desorption isotherms. Pores larger than 50 nm scatter visible light significantly and result in small transmittance and large haze [54]. The spectral transmittance of the aerogel film reached a maximum of 86% at 1100 nm but was equal on average to $\sim 60\%$ in the visible range (400–700 nm). The haze between 400 and 700 nm equals 83–74%, respectively. For applications where transparency in the visible range is required more work should be done to improve the pore size and homogeneity.

3.4. Thermal characterization

The thermal resistivity of the aerogel film was illustrated by imaging with an IR camera. Fig. 7 shows the aerogel film (thickness $\sim 130 \mu\text{m}$) and a reference polyimide (Kapton®) film of a comparable thickness ($\sim 130 \mu\text{m}$) on the surface of a hot plate. The films were placed simultaneously on the plate which was set to $100 \text{ }^\circ\text{C}$. After 1.5 min, the temperature at the surface of the aerogel film was $68 \text{ }^\circ\text{C}$ while the polyimide film was $84 \text{ }^\circ\text{C}$. The different temperatures observed for the two films correspond to the difference in their thermal conductivity. This qualitative test was repeated several times and similar images were obtained.

4. Conclusion

In view of the growing needs for efficient insulating porous materials in microsystems [7–12], we describe a new method for preparing aerogel films in liquid molds. Liquid molding offers an attractive alternative

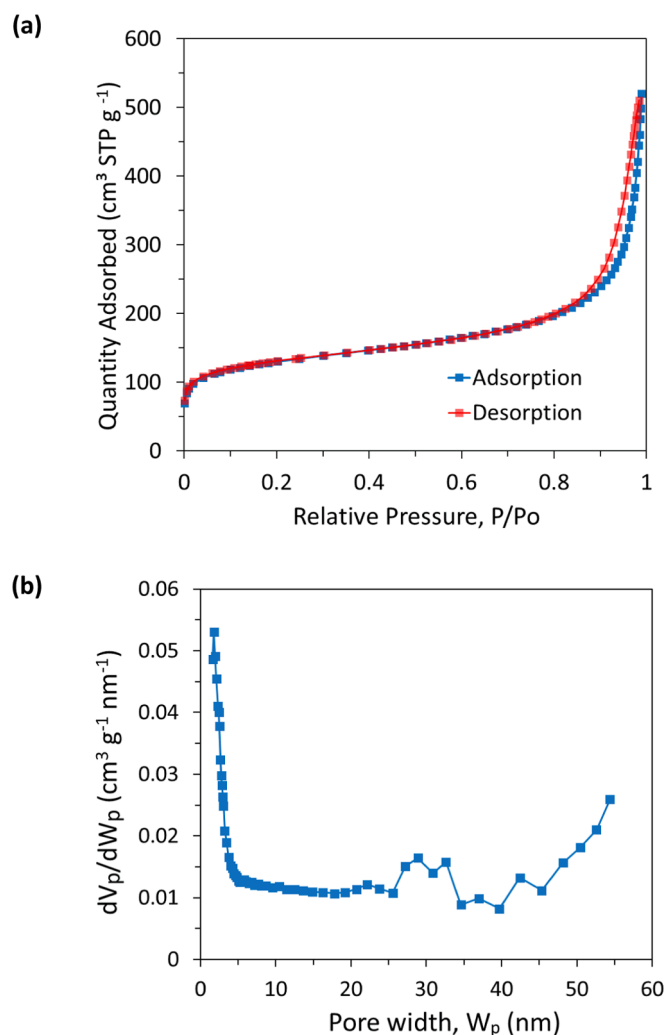


Fig. 5. (a) Nitrogen adsorption–desorption isotherm and (b) the corresponding mesopore size distribution of silica aerogel film synthesized in a liquid mold with fluorinert as the substrate and octanol as the cover.

Table 1

Summary of the structural characteristics of silica aerogel films synthesized in a liquid mold with fluorinert as a substrate and octanol as a cover.

BET Specific area ($\text{m}^2 \cdot \text{g}^{-1}$)	Porosity (%)	Total specific volume ($\text{cm}^3 \cdot \text{g}^{-1}$)	Micropore specific volume ($\text{cm}^3 \cdot \text{g}^{-1}$)	Mesopore specific volume ($\text{cm}^3 \cdot \text{g}^{-1}$)	Macropore specific volume ($\text{cm}^3 \cdot \text{g}^{-1}$)
430	91	4.81	0.05	0.40	4.36

to the currently used deposition methods, which are limited to production of very thin films ($<2 \mu\text{m}$) [17–19]. Furthermore, the aerogels produced in liquid molds are free-standing and the new approach is more efficient, economical, and environmentally friendly.

The liquid mold consists of two immiscible liquids with different densities, which are used as substrate and cover to encapsulate a sol during gelation and aging. While the gel is immersed between the liquids, it is fully protected from uncontrolled solvent evaporation. This overcomes the risk of shrinkage and cracking of the gel, preserving its fine porous structure. Moreover, the use of liquid molds allows for reduced friction and stress during gelation and results in smooth surfaces. Once gelation is completed, the liquids constituting the mold are washed away and the gel is dried under supercritical conditions with CO_2 . The liquids of the mold can be recovered following the synthesis for

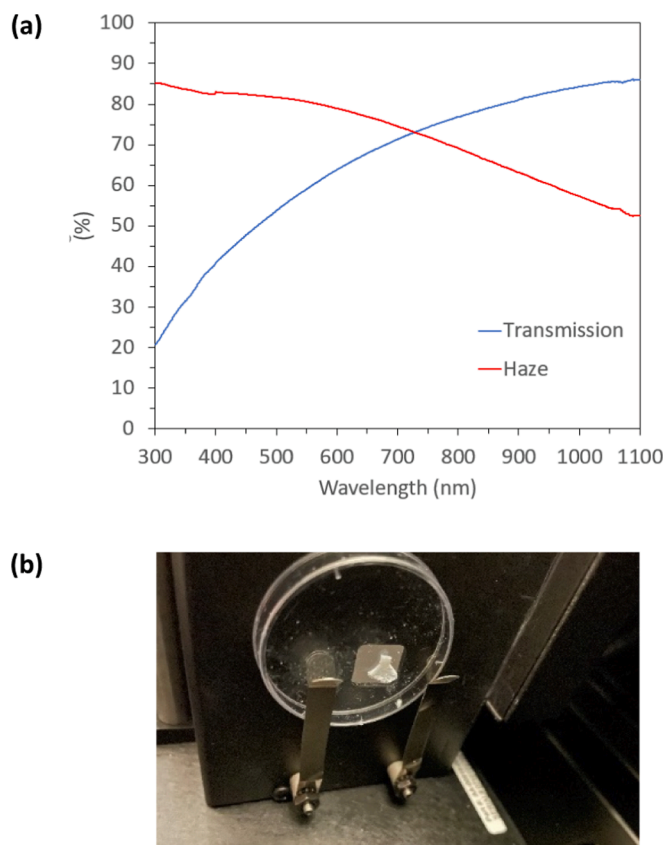


Fig. 6. (a) Spectral normal-hemispherical transmittance and haze as a function of wavelength between 300 and 1100 nm of a dry silica aerogel film with thickness $\sim 130 \mu\text{m}$. (b) Sample was held by electrostatic attraction on a polystyrene slide.

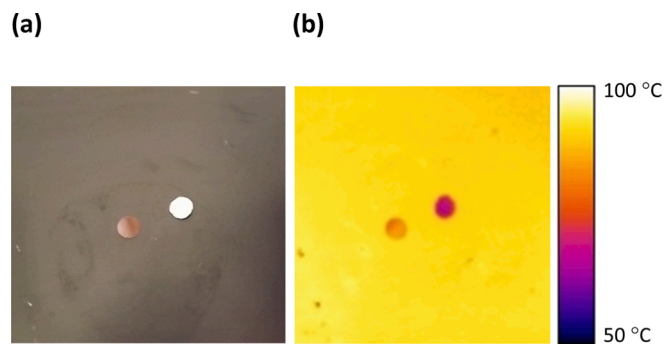


Fig. 7. (a) A picture of an aerogel film of $130 \mu\text{m}$ (white) next to a polyimide film of $130 \mu\text{m}$ (orange) on the surface of a hotplate. (b) IR image of the films taken after 1.5 min on a hot plate set at $100 \text{ }^\circ\text{C}$. (For interpretation of the references to colour in this figure legend, the reader is referred to the web version of this article.)

reuse in subsequent preparations.

Generally, the thickness of gels produced in liquid molds is determined by the surface tension between the liquids. Two model systems were tested as liquid molds for silica sols: (1) a liquid mold with silicone oil as a substrate and mineral oil as a cover; (2) a liquid mold with fluorine oil as a substrate and octanol as a cover. The first produced free standing lens shaped silica aerogels with a thickness of $\sim 4 \text{ mm}$. In the second, silica aerogel films with $130 \mu\text{m}$ thickness and 91% porosity were produced. The films specific surface area was $430 \text{ m}^2 \cdot \text{g}^{-1}$ with a broad pore size distribution consisting of micropores, mesopores, and

macropores. The relatively low transmission and high haze of the film are in line with the presence of large pores (>50 nm). The thermal conductivity of the films was demonstrated by IR imaging and showed better insulation than a polyimide film of similar thickness.

In future research liquid molding can be extended to colloidal solutions other than silica. This might be specifically beneficial for those containing highly volatile solvents and would entail specific matching of the liquids. An additional challenge would be to optimize the conditions required to obtain films with desired thicknesses. Liquid molds can also be used for shaping smooth spherical and aspherical optical components, as shown by Frumkin et al [55], or provide a means to control the assembly of colloidal solutions e.g. introduce different functionalities to opposite surfaces and generate films with specific directionality.

The similarity of the liquid mold method and the float glass technique supports the feasibility of mass production of large sheets of aerogel films. In fact, even in the absence of a dedicated set-up (vibration control, rigid support for handling etc.) we have successfully molded a large film (10 cm in diameter and 130 μm thick). Supporting the notion that floating gels can be rolled at a controlled speed between two flowing liquids to form large sheets of stand-alone aerogel films in a continuous process for mass production.

CRedit authorship contribution statement

Galit Bar: Conceptualization, Methodology, Formal analysis, Data curation, Visualization, Project administration, Writing – original draft, Funding acquisition. **Linoy Amar:** Investigation, Formal analysis. **Michal Marszewski:** Investigation, Formal analysis, Data curation, Writing – review & editing. **Assaf Bolker:** Investigation, Formal analysis, Data curation. **Ali Dashti:** Investigation, Formal analysis, Data curation. **Raphy Dror:** Formal analysis. **Laurent Pilon:** Methodology, Formal analysis, Project administration, Supervision, Writing – review & editing, Funding acquisition.

Declaration of Competing Interest

The authors declare that they have no known competing financial interests or personal relationships that could have appeared to influence the work reported in this paper.

Data availability

Data will be made available on request.

Acknowledgments

This work was supported in part by the Pazy Foundation of the Israeli Council for Higher Education, the Israel Atomic Energy Commission, and by the Advanced Research Projects Agency-Energy (ARPA-E) Single-Pane Highly Insulating Efficient Lucid Designs (SHIELD) program (ARPA-E Award DE-AR0000738). GB would like to thank the Pazy Foundation for a personal grant for her sabbatical year at UCLA. The authors would also like to thank (i) S. King and N. Kashanchi for their help with the ASAP measurements, (ii) T. Wright from the California NanoSystems Institute at UCLA, and (iii) G. Berkovic from NRC Soreq, and (iv) A. Navon from the Weizmann Institute of Science for helpful and fruitful discussions.

References

- [1] T.F. Baumann, A.E. Gash, G.A. Fox, J.H. Satcher, L.W. Hrubesh, Oxidic Aerogels, in: F. Schth, K.S.W. Sing, J. Weitkamp (Eds.), Handbook of Porous Solids, Wiley-VCH Verlag GmbH, Weinheim, Germany, 2002, pp. 2014–2037, <https://doi.org/10.1002/9783527618286.ch26a>.
- [2] M.A. Aegerter, N. Leventis, M.M. Koebel, eds., Aerogels Handbook, Springer New York, New York, NY, 2011. <https://doi.org/10.1007/978-1-4419-7589-8>.
- [3] P. Scheuerflug, M. Hauck, J. Fricke, Thermal properties of silica aerogels between 1.4 and 330 K, *J. Non Cryst. Solids* 145 (1992) 196–201, [https://doi.org/10.1016/S0022-3093\(05\)80455-7](https://doi.org/10.1016/S0022-3093(05)80455-7).
- [4] Stepanian Christopher J., Gould George L., Begag Redouane, Aerogel composite with fibrous batting, US7078359B2, 2006. <https://patentimages.storage.googleapis.com/e3/03/7b/edb2bf30d61754/US7078359.pdf>.
- [5] K.I. Jensen, J.M. Schultz, F.H. Kristiansen, Development of windows based on highly insulating aerogel glazings, *J. Non Cryst. Solids* 350 (2004) 351–357, <https://doi.org/10.1016/j.jnoncrysol.2004.06.047>.
- [6] Lumira® Aerogel, n.d. <https://solarinnovations.com/lumira-aerogel/#>.
- [7] M. Madani, D.R. Lankireddy, N.-F. Tzeng, Gaseous sensors with area- and energy-efficient microhotplates through silica aerogel for heat insulation, in: 2009 International Conference on Microelectronics - ICM, IEEE, Marrakech, Morocco, 2009; pp. 402–405. <https://doi.org/10.1109/ICM.2009.5418598>.
- [8] N. Kawakami, Y. Fukumoto, T. Kinoshita, K. Suzuki, K. Inoue, Preparation of Highly Porous Silica Aerogel Thin Film by Supercritical Drying, *Jpn. J. Appl. Phys.* 39 (2000) L182, <https://doi.org/10.1143/JJAP.39.L182>.
- [9] S. Reede, F. Bunge, M.J. Vellekoop, Integration of Silica Aerogels in Microfluidic Chips, in: Proceedings of Eurosensors 2017, Paris, France, 3–6 September 2017, MDPI, 2017; p. 298. <https://doi.org/10.3390/proceedings1040298>.
- [10] Shih-Kang Fan, Chang-Jin Kim, Jong-Ah Paik, B. Dunn, P.R. Patterson, M.C. Wu, MEMS with thin-film aerogel, in: Technical Digest. MEMS 2001. 14th IEEE International Conference on Micro Electro Mechanical Systems (Cat. No.01CH37090), IEEE, Interlaken, Switzerland, 2001; pp. 122–125. <https://doi.org/10.1109/MEMSYS.2001.906494>.
- [11] R. Yokokawa, J.-A. Paik, B. Dunn, N. Kitazawa, H. Kotera, C.-J. Kim, Mechanical properties of aerogel-like thin films used for MEMS, *J. Micromech. Microeng.* 14 (2004) 681–686, <https://doi.org/10.1088/0960-1317/14/5/004>.
- [12] C.-T. Wang, C.-L. Wu, Electrical sensing properties of silica aerogel thin films to humidity, *Thin Solid Films* 496 (2006) 658–664, <https://doi.org/10.1016/j.tsf.2005.09.001>.
- [13] C.J. Brinker, G.W. Scherer, Elsevier (Amsterdam), Sol-Gel Science: The Physics and Chemistry of Sol-Gel Processing, Elsevier Science, 1990. <https://books.google.co.il/books?id=V2vRvTsTaCwMC>.
- [14] G.W. Scherer, Theory of Drying, *J. Am. Ceram. Soc.* 73 (1990) 3–14, <https://doi.org/10.1111/j.1151-2916.1990.tb05082.x>.
- [15] A. Venkateswara Rao, D. Haranath, G.M. Pajonk, P.B. Wagh, Optimisation of supercritical drying parameters for transparent silica aerogel window applications, *Mater. Sci. Technol.* 14 (1998) 1194–1199, <https://doi.org/10.1179/mst.1998.14.11.1194>.
- [16] G.W. Scherer, Recent progress in drying of gels, *J. Non Cryst. Solids* 147–148 (1992) 363–374, [https://doi.org/10.1016/S0022-3093\(05\)80645-3](https://doi.org/10.1016/S0022-3093(05)80645-3).
- [17] L.W. Hrubesh, J.F. Poco, Thin aerogel films for optical, thermal, acoustic and electronic applications, *J. Non Cryst. Solids* 188 (1995) 46–53, [https://doi.org/10.1016/0022-3093\(95\)00028-3](https://doi.org/10.1016/0022-3093(95)00028-3).
- [18] M. Seyedjalali, S. Kumar, M.R. Madani, Ultra-dense and ultra-low power microhotplates using silica aerogel, *Electron. Lett.* 49 (2013) 1168–1170, <https://doi.org/10.1049/el.2013.1389>.
- [19] M.-H. Jo, J.-K. Hong, H.-H. Park, J.-J. Kim, S.-H. Hyun, Evaluation of SiO₂ aerogel thin film with ultra low dielectric constant as an intermetal dielectric, *Microelectron. Eng.* 33 (1997) 343–348, [https://doi.org/10.1016/S0167-9317\(96\)00063-9](https://doi.org/10.1016/S0167-9317(96)00063-9).
- [20] Pilkington, Lionel A. B., Manufacture of flat glass, US Patent 2,911,759, 1959. <http://patents.google.com/patent/US2911759A/en>.
- [21] Kazaura Najib, Latest Development and architectural applications of float glass, (2014). https://www.academia.edu/8726675/Latest_Developments_and_Architectural_Applications_Of_Float_Glass.
- [22] E.M. Rabinovich, D.W. Johnson Jr., A. Mishkevich, E.A. Chandross, J. Thomson Jr., Sol-Gel Particulate Float Process to Make Vitreous Silica Bodies, *J. Sol-Gel Sci. Technol.* 28 (2003) 19–29, <https://doi.org/10.1023/A:1025624801014>.
- [23] M. Marszewski, S.C. King, Y. Yan, T. Galy, M. Li, A. Dashti, D.M. Butts, J.S. Kang, P. E. McNeil, E. Lan, B. Dunn, Y. Hu, S.H. Tolbert, L. Pilon, Thick Transparent Nanoparticle-Based Mesoporous Silica Monolithic Slabs for Thermally Insulating Window Materials, *ACS Appl. Nano Mater.* 2 (2019) 4547–4555, <https://doi.org/10.1021/acsnm.9b00903>.
- [24] Y. Song, J.-B. Fan, S. Wang, Recent progress in interfacial polymerization, *Mater. Chem. Front.* 1 (2017) 1028–1040, <https://doi.org/10.1039/C6QM00325G>.
- [25] M. Yamane, S. Shibata, A. Yasumori, T. Yano, S. Uchihiro, Thick silicate glass film by an interfacial polymerization: Code E2, *J. Sol-Gel Sci Technol.* 2 (1994) 457–460, <https://doi.org/10.1007/BF00486290>.
- [26] N.E. Chayen, A novel technique for containerless protein crystallization, *Protein Eng Des Sel.* 9 (1996) 927–929, <https://doi.org/10.1093/protein/9.10.927>.
- [27] N.E. Chayen, The role of oil in macromolecular crystallization, *Structure* 5 (1997) 1269–1274, [https://doi.org/10.1016/S0969-2126\(97\)00279-7](https://doi.org/10.1016/S0969-2126(97)00279-7).
- [28] Stephen Steiner, Aerogel.org, (n.d.). <http://www.aerogel.org/>.
- [29] S. Kim, J. Chen, T. Cheng, A. Gindulyte, J. He, S. He, Q. Li, B.A. Shoemaker, P.A. Thiessen, B. Yu, L. Zaslavsky, J. Zhang, E.E. Bolton, PubChem 2023 update, *Nucleic Acids Res.* 51 (2023) D1373–D1380. <https://doi.org/10.1093/nar/gkac956>.
- [30] M.J. Rosen, Wetting and Its Modification by Surfactants, in: Surfactants and Interfacial Phenomena, 3. ed, Wiley-Interscience, Hoboken, NJ, 2004; pp. 243–276.
- [31] W.D. Harkins, A. Feldman, Films. The Spreading of Liquids and the Spreading Coefficient, *J. Am. Chem. Soc.* 44 (1922) 2665–2685. <https://doi.org/10.1021/ja01433a001>.

- [32] J. Noh, S. Jeong, J.-Y. Lee, Ultrafast formation of air-processable and high-quality polymer films on an aqueous substrate, *Nat Commun.* 7 (2016) 12374, <https://doi.org/10.1038/ncomms12374>.
- [33] J.C. Burton, F.M. Huisman, P. Alison, D. Rogerson, P. Taborek, Experimental and Numerical Investigation of the Equilibrium Geometry of Liquid Lenses, *Langmuir* 26 (2010) 15316–15324, <https://doi.org/10.1021/la102268n>.
- [34] I. Langmuir, Oil Lenses on Water and the Nature of Monomolecular Expanded Films, *J. Chem. Phys.* 1 (1933) 756–776, <https://doi.org/10.1063/1.1749243>.
- [35] P.R. Pujado, L.E. Scriven, Sessile lenticular configurations: Translationally and rotationally symmetric lenses, *J. Colloid Interface Sci.* 40 (1972) 82–98, [https://doi.org/10.1016/0021-9797\(72\)90175-0](https://doi.org/10.1016/0021-9797(72)90175-0).
- [36] H. Charnock, The float glass process, *Phys. Bull.* 21 (1970) 153–156, <https://doi.org/10.1088/0031-9112/21/4/018>.
- [37] F. Eslami, J.A.W. Elliott, Gibbsian Thermodynamic Study of Capillary Meniscus Depth, *Sci Rep.* 9 (2019) 657, <https://doi.org/10.1038/s41598-018-36514-w>.
- [38] Wayne Rasband, ImageJ, (2020).
- [39] S. He, H. Yang, X. Chen, Facile synthesis of highly porous silica aerogel granules and its burning behavior under radiation, *J Sol-Gel Sci Technol.* 82 (2017) 407–416, <https://doi.org/10.1007/s10971-017-4304-4>.
- [40] L. Juhász, K. Moldován, P. Gurikov, F. Liebner, I. Fábrián, J. Kalmár, C. Cserhádi, False Morphology of Aerogels Caused by Gold Coating by SEM Imaging, *Polymers* 13 (2021) 588, <https://doi.org/10.3390/polym13040588>.
- [41] S. Brunauer, P.H. Emmett, E. Teller, Adsorption of Gases in Multimolecular Layers, *J. Am. Chem. Soc.* 60 (1938) 309–319, <https://doi.org/10.1021/ja01269a023>.
- [42] S. Lowell, J.E. Shields, M.A. Thomas, M. Thommes, Characterization of Porous Solids and Powders: Surface Area, Pore Size and Density, Springer, Netherlands, Dordrecht (2004), <https://doi.org/10.1007/978-1-4020-2303-3>.
- [43] E.P. Barrett, L.G. Joyner, P.P. Halenda, The Determination of Pore Volume and Area Distributions in Porous Substances. I. Computations from Nitrogen Isotherms, *J. Am. Chem. Soc.* 73 (1951) 373–380, <https://doi.org/10.1021/ja01145a126>.
- [44] M. Kruk, M. Jaroniec, A. Sayari, Application of Large Pore MCM-41 Molecular Sieves To Improve Pore Size Analysis Using Nitrogen Adsorption Measurements, *Langmuir* 13 (1997) 6267–6273, <https://doi.org/10.1021/la970776m>.
- [45] M. Jaroniec, L.A. Solovoyov, Improvement of the Kruk–Jaroniec–Sayari Method for Pore Size Analysis of Ordered Silicas with Cylindrical Mesopores, *Langmuir* 22 (2006) 6757–6760, <https://doi.org/10.1021/la0609571>.
- [46] Rouquerol Françoise, Rouquerol Jean, Sing Kenneth, Adsorption by Powders and Porous Solids, Elsevier, 1999. <https://doi.org/10.1016/B978-0-12-598920-6.X5000-3>.
- [47] Standard Test Method for Haze and Luminous Transmittance of Transparent Plastics, American Society for Testing Materials, 2010. <https://www.astm.org/d1003-00.html>.
- [48] H. Yoo, H. Park, S. Yoo, S. On, H. Seong, S.G. Im, J.-J. Kim, Highly stacked 3D organic integrated circuits with via-hole-less multilevel metal interconnects, *Nat Commun.* 10 (2019) 2424, <https://doi.org/10.1038/s41467-019-10412-9>.
- [49] S.W. Fong, C.M. Neumann, E. Yalon, M.M. Rojo, E. Pop, H.-S.-P. Wong, Dual-Layer Dielectric Stack for Thermally Isolated Low-Energy Phase-Change Memory, *IEEE Trans. Electron Devices.* 64 (2017) 4496–4502, <https://doi.org/10.1109/TED.2017.2756071>.
- [50] A.S. Shalygin, A.L. Nuzhdin, G.A. Bukhtiyarova, O.N. Martyanov, Preparation of HKUST-1@silica aerogel composite for continuous flow catalysis, *J Sol-Gel Sci Technol.* 84 (2017) 446–452, <https://doi.org/10.1007/s10971-017-4455-3>.
- [51] S. Zong, W. Wei, Z. Jiang, Z. Yan, J. Zhu, J. Xie, Characterization and comparison of uniform hydrophilic/hydrophobic transparent silica aerogel beads: skeleton strength and surface modification, *RSC Adv.* 5 (2015) 55579–55587, <https://doi.org/10.1039/C5RA08714G>.
- [52] M. Thommes, K. Kaneko, A.V. Neimark, J.P. Olivier, F. Rodriguez-Reinoso, J. Rouquerol, K.S.W. Sing, Physisorption of gases, with special reference to the evaluation of surface area and pore size distribution (IUPAC Technical Report), *Pure Appl. Chem.* 87 (2015) 1051–1069, <https://doi.org/10.1515/pac-2014-1117>.
- [53] A. Sedova, G. Bar, O. Goldbart, R. Ron, B. Achrai, I. Kaplan-Ashiri, V. Brumfeld, A. Zak, R. Gvishi, H.D. Wagner, R. Tenne, Reinforcing silica aerogels with tungsten disulfide nanotubes, *J. Supercrit. Fluids* 106 (2015) 9–15, <https://doi.org/10.1016/j.supflu.2015.07.018>.
- [54] J. Wang, D. Petit, S. Ren, Transparent thermal insulation silica aerogels, *Nanoscale Adv.* 2 (2020) 5504–5515, <https://doi.org/10.1039/D0NA00655F>.
- [55] V. Frumkin, M. Bercovici, Fluidic shaping of optical components, *Flow.* 1 (2021) E2, <https://doi.org/10.1017/flo.2021.1>.